Interactions of Inter- and Intraphase Gradients in a Diffusion Limited Catalytic Reaction

J. P. G. KEHOE and J. B. BUTT

Department of Engineering and Applied Science
Yale University, New Haven, Connecticut 06520

The experimental measurement of inter- and intraphase temperature gradients in a single pellet reactor for the Ni-kieselguhr catalyzed benzene hydrogenation reaction is described. Experimental variables were temperature, feed composition, flow rate (hence heat and mass transfer coefficients) and intrinsic catalytic activity. All parameters required for carrying out calculations were either measured in separate experiments or compared with available independent information. The rather complex interactions between inter- and intraphase gradients are well represented by the theory except at conditions of high reaction rate and low convective transport rate. The discrepancies observed at these conditions are apparently due to the development of nonuniform external boundary layers.

We have previously reported experimental measurements of intraparticle temperature gradients in the supported nickel catalyzed benzene hydrogenation reaction (*1*). These together with other measurements (*2* to *5*) indicate that considerable intraphase gradients occur and are reconcilable with existing theory in some respects. Several items, however, remain to be resolved. In the first instance, stated agreement of theory with experiment has been obtained by adjustment of parametric values to obtain best fit, rather than by separate parametric evaluation before carrying out calculations. Secondly, a number of recent studies (*6* to *10*) have been concerned with the interactions of intra- and interphase gradients, particularly in exothermic reaction systems. Most work to date has been carried out for models where surface concentration and temperature are specified, although in fact it has been shown clearly that if internal gradients of temperature exist, external gradients must also exist (*6, 11*). The effect of external gradients on overall behavior is quite significant.

The objectives of the present study are twofold; measurement of both internal and external temperature gradients in a diffusion limited exothermic reaction, and comparison of such results with the predictions of theory based on separately measured parameter values. The reaction and catalyst is that reported by Irving and Butt (*1*); however, a modified single pellet reactor system has been employed to facilitate measurement of external gradients, as described subsequently. Similar experimentation has been reported by Hughes and Koh (*5*) for the ethylene hydrogenation reaction, but the uniform external temperature permitted by the current reactor design, which allows direct comparison of theory and experiment, is not obtained with the annular, axial flow reactor (*1, 5*). The need for independent parameter values requires a detailed investigation of the kinetics of benzene hydrogenation at low temperatures. This is reported elsewhere (*12*).

Correspondence concerning this paper should be addressed to J. B. Butt at Northwestern University, Evanston, Illinois 60201. J. P. G. Kehoe is at University College, Dublin, Ireland.

MODELING THE EXPERIMENTAL SYSTEM

The experimental reactor system is designed to conform to an infinitely long cylinder of porous catalytic material with a gas stream flowing transverse to the cylindrical axis supplying reactants and removing products. The major assumptions are those of uniform boundary layer, radial symmetry, homogeneity of the porous structure, and independence of temperature fields from angular or axial position. The kinetics employed involve the form determined specifically for this system (*12*), under conditions of low temperature and high hydrogen partial pressure, that is,

$$r = \frac{A \exp(-E/RT)C}{1 + B \exp(H/RT)C} \tag{1}$$

The conservation equations, using effective transport coefficients, assume the following nondimensional forms under conditions of excess hydrogen:

$$\frac{\partial^2 y}{\partial z^2} + \frac{1}{z}\frac{\partial y}{\partial z} - \frac{\delta e^{\gamma(1-1/\theta)} y}{1 + \alpha e^{\xi/\theta} y} = 0 \tag{2}$$

$$\frac{\partial^2 \theta}{\partial z^2} + \frac{1}{z}\frac{\partial \theta}{\partial z} + \frac{\beta\delta e^{\gamma(1-1/\theta)} y}{1 + \alpha e^{\xi/\theta} y} = 0 \tag{3}$$

with the boundary conditions

$$\frac{d\theta}{dz} = \frac{dy}{dz} = 0 \quad ; \quad z = 0$$

$$\frac{d\theta}{dz} = N_{Nu}(1 - \theta_S) \quad ; \quad z = 1 \tag{4}$$

$$\frac{dy}{dz} = N_{Sh}(1 - y_S) \quad ; \quad z = 1$$

This set is solved numerically using the Thomas method; complete details of the technique and solution procedure are given by Kehoe (*13*). For a radial grid of 101 points converged solutions were obtained in approximately four seconds (IBM 7090).

The effectiveness factor as reported subsequently is the ratio of the observed rate to the intrinsic rate at bulk conditions. In terms of the nondimensional variables above

$$\eta = \frac{2N_{Sh}\,(1 - y_S)\,[1 + \alpha e^{\xi}]}{\delta} \qquad (5)$$

EXPERIMENT

Materials. The catalyst was nickel-kieselguhr in the form of a powder, Harshaw Ni-0104P. Metal content is 58% by weight, powder surface area is 150 sq.m./g. and average pore radius 37 Å. In some experiments a diluted catalyst was employed, consisting of two parts alumina (Harshaw Al-0104T), one part graphite (flake graphite from Dixon Graphite Company degassed at high temperature) and one part Ni-kieselguhr.

Pure gases were supplied by Air Products Company; prepurified nitrogen and helium were further dried in beds of molecular sieves, and prepurified H_2 was treated for removal of oxygen in a commercial deoxo unit and dried over anhydrous calcium sulfate.

Spectrometer grade benzene from Fisher Scientific Company, redistilled for removal of trace thiophene, was used in all experiments.

Reactor and Flow Systems. The overall flow system employed was a modification of that described by Irving and Butt. The specially designed single pellet reactor is shown on Figure 1. The test cylindrical catalyst pellet is supported vertically between two teflon plugs in a stainless steel tube; reactor feed enters through two slots in the side of the containing tube running the length of the pellet, and effluent departs via two similar slots positioned at right angles to the inlets. Four thermocouples are positioned across the diameter of the pellet (*1*) at approximately the center of the reactor; these were iron-constantan, .002-in. diam., supplied by Omega Engineering Company. The pellet thermocouples were welded to 24-gauge lead wires enclosed in fibreglass insulation connected to external circuits. Bulk gas temperatures were also determined by an iron-constantan thermocouple positioned as shown. The reactor was enclosed in an air bath which permitted control of surroundings temperature to ±0.1°C.

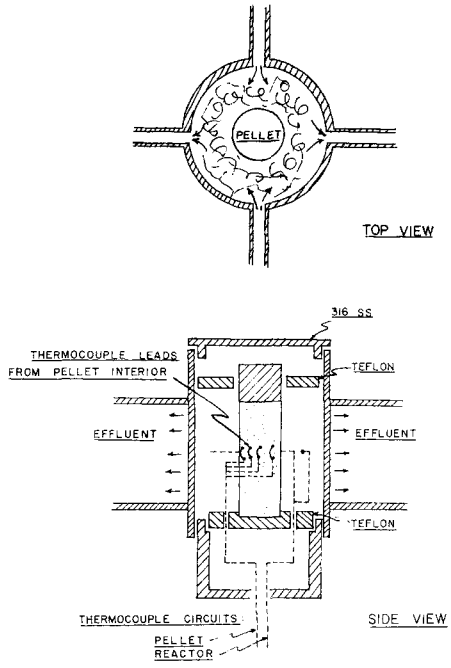

Fig. 1. The single pellet reactor.

Ancillary Equipment. Nitrogen adsorption-desorption isotherms for characterization of the catalyst pellets were obtained with a commercial sorptometer. Composition analysis was conducted by GC with thermal conductivity detection. The thermal conductivity of catalyst pellets was measured with a Colora thermoconductometer, Colora Messtecknik, Wuttemberg, using a comparative method relative to standard glass samples.

Operation. Catalyst Pretreatment consisted of passing hydrogen, at a rate of 100 cu.cm./min. for 1 hr. and 200 cu.cm./min. for a minimum of 12 additional hr., at 120°C. through the reactor containing the test pellet. This process was repeated between each series of runs, and yielded a stable and reproducible catalyst activity with the redistilled benzene feed. On completion of pretreatment, hydrogen, and benzene flows were established in the bypass system and after flow stabilisation the bypass was closed and the total flow, mixed feed introduced to the reactor. Flow rates employed were 5, 10, or 15 liter/min. and steady state conditions were attained within 15 min. in all experiments. The primary experimental values measured were flow and composition of feed, composition of reactor effluent, and temperatures of feed, reactor bulk gas phase, and within the particle.

RESULTS

For the undiluted catalyst (Pellet 1) feed temperatures were kept below 65°C. to avoid temperatures within the pellet beyond the region of the validity of the kinetic interpretation (~200°C.). Temperatures of 26, 52, and 65°C. were employed and at each level experiments were conducted at flow rates of 5, 10, and 15 liter/min. with benzene feed concentrations varying between 0 and 15 mole %. The dilute catalyst (Pellet 2) permitted higher temperatures, and experiments were conducted at 55, 67, 85, and 134°C. with the same range of flow rate and benzene concentration. A summary of experimental conditions is given by Kehoe (*13*).

In most experiments the rate of heat generation was sufficiently large to raise reactor bulk gas temperatures above that of the air bath. As the flow rate increased this difference decreased, and the change in reactor temperature at different flow rates can be correlated with the measured rate, as shown in Figure 2a.

Kinetics. The kinetics of the hydrogenation were determined separately for these catalysts at the conditions (temperatures to 150°C., atmospheric total pressure, $H_2/C_6H_6 \sim 10$) employed in the pellet reactor. These were correlated with the rate law of Equation (1) and the following parametric values (*12*):

$$A/\rho_H = 1.57 \times 10^{-6}\ \text{g.-moles } C_6H_6/(\text{g.-cat.})(\text{sec.})(\text{torr})^2 \quad \text{(Pellet 1)}$$

$$B = 8.9 \times 10^{-6}\ \text{torr}^{-1}$$

$$E = 12.29\ \text{kcal./mole}$$

$$H = 8.26\ \text{kcal./mole}$$

These values fit measured rates to within 10% in all cases, and generally to about 5%. The dilution to make Pellet 2 produced a linear response in the kinetics, so that A/ρ_H for this pellet was 0.25 in the value above.

Characterization of the Catalytic System. As discussed above, it was desired to determine by separate experiments, or other means independent of fitting calculations to experimental profiles, all the parameters characterizing the system. In Table 1 is given a tabulation of these parameters for the present study, and the following gives a brief description of the means employed for their determination.

1. Density and density homogeneity were determined gravimetrically using measured pellet volume. Used pellets were sectioned into three pieces for measurement of the axial density homogeneity.

2. Pellet heat capacities were estimated from the specific heats of the individual components, as given in the International Critical Tables, and the composition.

3. Effective thermal conductivity was measured separately using the thermoconductometer. The conductivity of Pellet 2 is an order of magnitude larger than that of Pellet 1, due to the inclusion of graphite, so a wide range of thermal parameters is encompassed by the two pellets.

4. Effective diffusivities have been measured previously for this catalyst using helium-argon (*14*), and such values can be corrected for molecular weight change to give an estimate for the present experiment. Alternatively, D_e can be obtained from the maximum intraparticle temperature rise in the steady state

$$D_e = \frac{\lambda_e(\Delta T)_{\max}}{C_S(-\Delta H)} \tag{6}$$

where C_S is the reactant concentration at the surface. A comparison was made between estimates of D_e; the difference in the worst case was less than 30% between the two sources. The value in Table 1 is representative for the experimental conditions.

5. Film heat transfer coefficients were determined directly from the data. Measured intraparticle profiles were used to establish surface temperatures and the heat transfer coefficient computed from the rate of reaction and the difference between bulk gas and surface temperature. This involves an extrapolation for surface temperature; however, the risks associated with this were minimized by using only runs where small extrapolations were required. An excellent linear correlation between ΔT and the rate of reaction was obtained, Figure 2b, and the heat transfer coefficient was calculated from

$$h = \frac{a(-\Delta H)\ (r)}{2(T_S - T_B)} \tag{7}$$

Values of h, with corresponding Nusselt numbers computed from the effective thermal conductivity, are given in Table 1. Heat transfer coefficients are approximately proportional to the square root of gas velocity, consistent with other findings, and are of the same magnitude as reported by Maymo and Smith (3) at somewhat lower flow rates in a similar configuration.

6. Mass transfer coefficients and Sherwood numbers were determined from the transport coefficients and gas density and heat capacity, using the approximation suggested by Carberry (6):

$$\frac{N_{Sh}}{N_{Nu}} \approx \frac{1}{\rho_G c_{pG}} \cdot \frac{\lambda_e}{D_e} \tag{8}$$

Typical values in this study are $\rho_G = 5.14 \times 10^{-4}$ g./cu.cm., c_{pG} of 0.65 cal./g.-°C., and λ_e and D_e as reported in Table 1. From these values $N_{Sh} \approx 20\ N_{Nu}$, as reported in the table.

7. The pore size distribution of Pellet 1 is bimodal, with a micropore porosity of 0.21 and average pore radius of 37Å. and macropore porosity of 0.29 and average pore radius of 4000Å. Total surface area of Pellet 1 is 129 sq.m./g.

Table 1. Parameters of the Catalyst Pellets Employed in the Experiments

Property	Pellet 1 Harshaw Ni-0104*P*, 58% Ni on kieselguhr	Pellet 2 25% Ni-0104*P*, 25% graphite, 50% γ-Al_2O_3 (Harshaw Al-0104*T*)
Pellet radius, cm.	0.66	0.69
Density, g./cu.cm	1.88	1.57
Length, cm.	5.75	6.10
Axial density homogeneity	±1.2%	±2.0%
Heat capacity, cal./(g.)(°C.)	0.152	0.187
Eff. thermal cond., cal./(cm.)(sec.)(°C.)	3.6×10^{-4}	3.5×10^{-3}
Eff. diffusivity, sq.cm./sec.	0.052	0.035
Heat transfer coeff., cal./(sq. cm.)(sec.)(°C.)		
(a) 5 liters/min. flow	9.35×10^{-3}	9.35×10^{-3}
(b) 10 liters/min. flow	13.1×10^{-3}	13.1×10^{-3}
(c) 15 liters/min. flow	16.2×10^{-3}	16.2×10^{-3}
Nusselt number $= ha/\lambda_e$		
(a)	17.2	1.7
(b)	24.0	2.4
(c)	29.7	3.0
Sherwood number $= k_m a/D_e$		
(a)	343	515
(b)	480	720
(c)	595	892

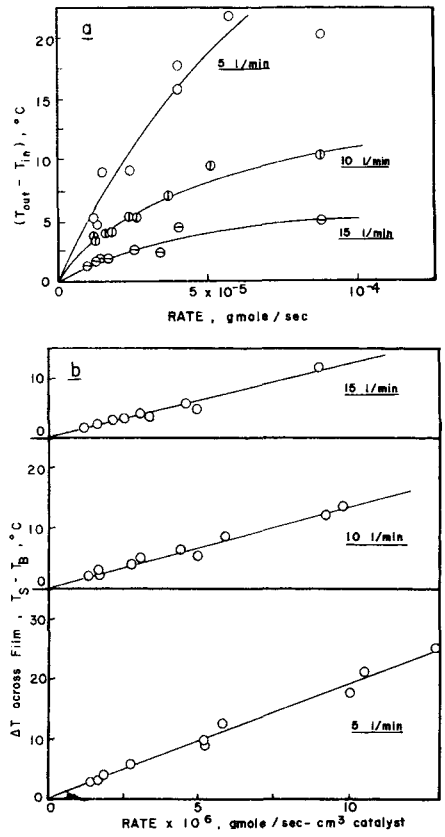

Fig. 2. *(a)*. Bulk gas temperature rise versus rate of reaction. *(b)*. Interphase temperature gradient as a function of rate of reaction.

Profile Measurements for Pellet 1

The steady state temperature profiles, determined by the primary variables of flow rate, feed composition, and feed temperature illustrate very well the complex interactions between internal and external transport resistances. At the lowest rate benzene is usually depleted in a thin annular shell of the catalyst particle; only a small internal gradient

is noted and the preponderant resistance is in the boundary layer. At higher flow rates, somewhat unexpectedly, this effect becomes much less pronounced.

At the lowest feed temperature 26°C. the feed composition was restricted to below 7% C_6H_6 to avoid condensation; the resulting low rates of reaction produced small gradients, both internal and external. Typical data are shown on Figure 3 for a benzene feed concentration of 2.2%. Measurements at other conditions at this temperature were similar.

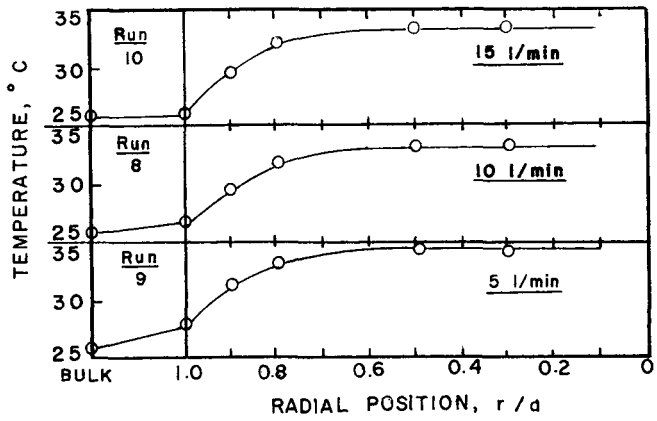

Fig. 3. Measured internal and external profiles for Pellet 1 with feed temperature of 26°C.

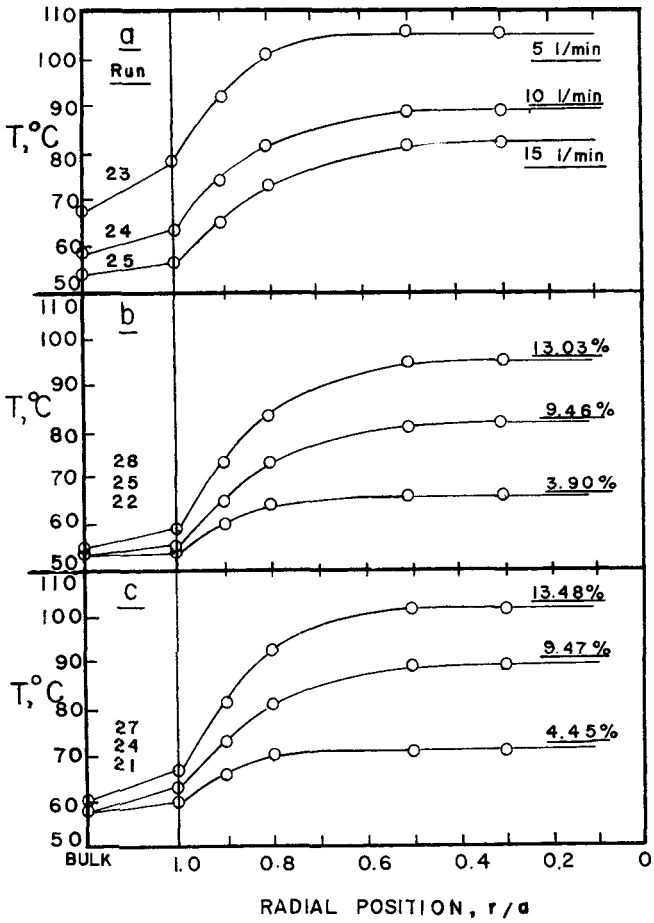

Fig. 4. Measured internal and external profiles for Pellet 1 with feed temperature of 52°C. (a). Profiles as a function of flow rate for feed composition of ~ 10% C_6H_6. (b). Profiles as a function of feed composition at high flow, 15 liters/min. (c). Profiles as a function of feed composition at intermediate flow, 10 liters/min.

Higher feed concentrations were permissible at 52°C. For example, at a flow of 5 liters/min. and composition of 10% the internal gradient was approximately 25°C., the external gradient 10°C., and the steady state bulk temperature 18°C. higher than the feed. At low flow rates it would be expected that most reaction occurs near the catalyst surface, and on increasing flow the zone of reaction penetrates more deeply into the pellet while becoming more diffuse. Experimental results confirming this are shown on Figure 4a. The effects of benzene feed concentration in this regard are less pronounced. Taking the flat portion of the internal temperature profile to correspond exactly to the region of complete reactant depletion would indicate that the reaction zone penetration increases with feed concentration at high flow rate (15 liters/min., Figure 4b) and is essentially stationary at lower flow rates (10 liters/min., Figure 4c). In fact, one would expect the reaction zone penetration to decrease with increasing concentration

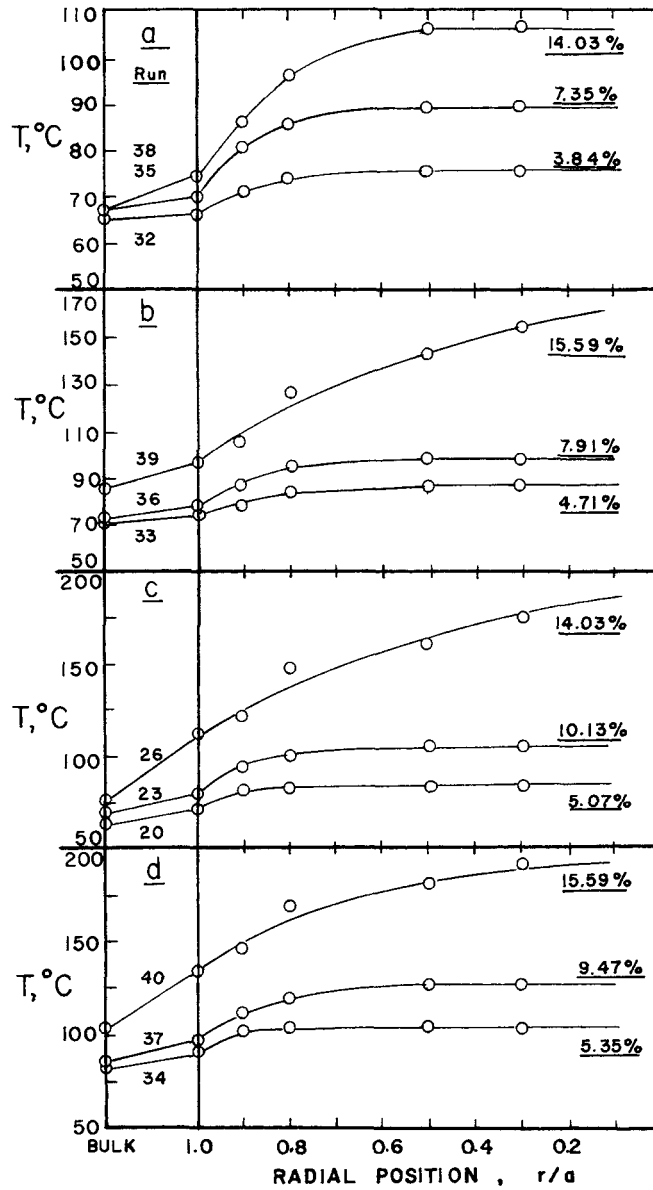

Fig. 5. Measured internal and external profiles for Pellet 1 with feed temperature of 52° and 65°C. (a). Profiles as a function of feed composition at flow of 15 liters/min., $T_F = 65$°C. (b). Profiles as a function of feed composition at flow of 10 liters/min., $T_F = 65$°C. (c). Profiles as a function of feed composition at flow of 5 liters/min., $T_F = 52$°C. (d). Profiles as a function of feed composition at flow of 5 liters/min., $T_F = 65$°C.

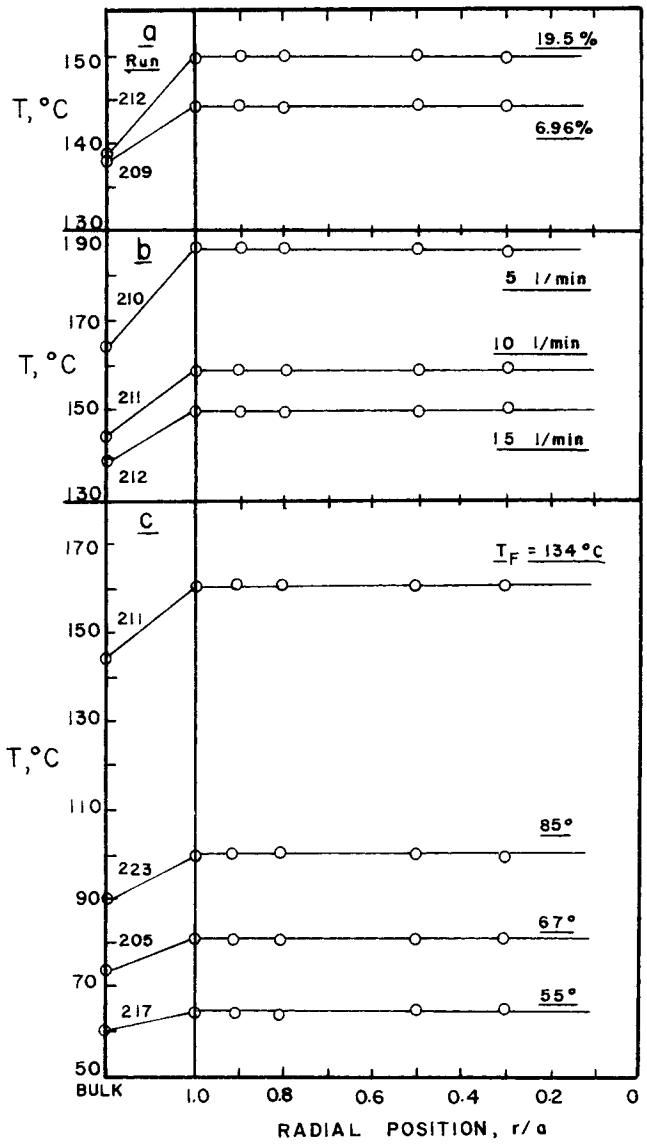

Fig. 6. Measured internal and external profiles for Pellet 2. *(a)*. Profiles as a function of feed composition. *(b)*. Profiles as a function of flow rate. *(c)*. Profiles as a function of feed temperature.

in accordance with the Prater relationship; this is not evident from the data of Figure 4b and c because (i) the isothermal zone and the zone of no reaction do not coincide, and (ii) the feed concentration effect is apparently not a strong one over the range of conditions employed here.

At 65°C. results at high flow rates are in accord with the 52°C. data. The effect of increasing concentration at total flows of 10 and 15 liters/min. is shown on Figure 5a and 5b. At the highest concentration of 15.6%, however, there is no isothermal zone within the pellet at the lower flow rate, contradictory to results at 52°C. This behavior appears characteristic of low flow rates and high reactant concentrations; on Figures 5c and 5d are profiles measured at 5 liters/min. for a range of feed compositions at both 52 and 65°C. These very large gradients are associated with high rates of reaction (for example, change from 10 to 15% C_6H_6 in Figure 5d yields a more than threefold increase in reaction rate) and, as shall be seen subsequently, are indeed not in accord with results at less severe conditions.

In the profile representations of Figures 3 to 5 the external gradient is represented by a linear segment over an arbitrary distance at the left of the figure. These gradients are determined from the measured overall rate of reaction and the correlation of Figure 2.

Profile Measurements for Pellet 2

While rates of reaction were far smaller on this pellet for equivalent conditions, the nearly ten-fold increase in thermal conductivity gave essentially isothermal intraparticle conditions. The maximum possible internal gradients were estimated to be about 2°C., and the greatest observed value was 1°C., which was within experimental error. Typical observations with Pellet 2 are summarized in Figure 6a, variation with feed composition at constant temperature and flow; Figure 6b, variation with flow rate at constant temperature and (approximately) feed composition; and Figure 6c, variation with temperature level with constant flow and feed composition.

Overall Rates of Reaction

It is of interest to examine the combined effects of all gradients on the overall rates of reaction. For Pellet 1 at 26°C. the reaction was sufficiently slow that external resistances were small and rates were independent of flow rate. Pore diffusion was important, however, and the rate increased with increasing benzene concentration, Figure 7a. Comparison of the measured rate with that computed from Equation (1) for bulk conditions gives effectiveness factors ranging up to 1.5 in some cases.

At higher temperatures both flow rate and benzene concentration affected the rate significantly. Rates at low concentrations were independent of flow over a small range, but as feed concentration was increased the pellet temperature increased considerably and external gradients became more important. At low flow rates, in particular, the heat generated was not removed by convection and intraparticle gradients became quite large. This is illustrated for the 52°C. feed temperature runs on Figure 7b, where the maximum temperature measured in the pellets is noted beside some of the points. Effectiveness at these higher

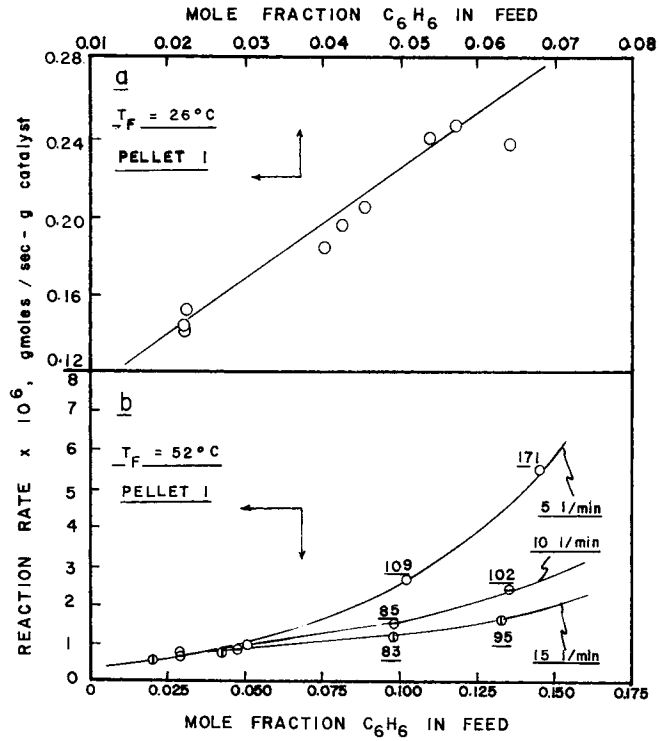

Fig. 7. Observed overall reaction rate as a function of flow rate and feed composition.

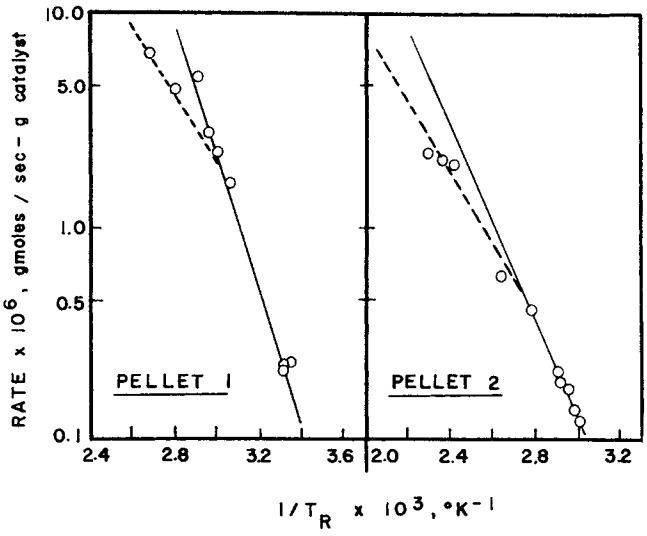

Fig. 8. Arrhenius plots of rate data with bulk reactor temperature.

temperatures was also generally greater than unity. Similar observations pertain for the rates measured with Pellet 2.

Apparent activation energies also reflect the interaction of the transport limits in the nonisothermal system. On Figure 8 are plotted in Arrhenius form the rates versus bulk temperature for measurements on both pellets. The apparent activation energy, determined from the limiting slope at low temperatures is 13.5 kcal./mole for Pellet 1 and 12.4 kcal./mole for Pellet 2. When surface temperatures are employed the results are 12.25 and 12.22, respectively, close to the independently determined value of 12.29 kcal./mole. At low temperatures the internal gradients for Pellet 1 are less than 5°C. and for Pellet 2 less than 1°C.; experimental effectiveness factors are in the range 1.0 to 1.1. At the higher temperatures shown on Figure 8 there is a significant decrease in the apparent activation energy, in accord with expectations based on increasing transport limits in the system. While the range of temperature involved in the experimentation is really not large enough for a detailed analysis, the apparent activation energies in the higher temperature regions, determined from the dotted lines in Figure 8, are about 6 kcal./mole in both cases. When external gradients are important, however, recall that decreasing activation energy by half is no longer a valid limiting rule for diffusion effects (6, 8).

COMPARISON WITH CALCULATION

For solution of Equations (2) to (4) we require values for the kinetic constants α and ξ, the activation energy parameter γ, the Thiele modulus φ (or δ, where $\delta = \varphi^2$), and the thermicity parameter β, in addition to the Nusselt and Sherwood numbers. All can be determined from the accumulation of kinetic data, the properties listed in Table 1, heats of reaction and heat capacity data, and the experimental conditions. A choice exists for the thermicity parameter β, since it can be conveniently related to the maximum particle temperature rise observed‡ as well as be determined independently. There is little difference between values of β determined by the two methods; the former, however, can account for small variations in effective transport properties caused by changes in experimental conditions not anticipated in our independent measurements and computations reported here employ this value of β. Values of the parameters for each of the experiments selected for illustration are given in Table 2.

Profiles

Predicted profiles for a number of experimental examples are given on Figures 9 and 10 in terms of dimensionless temperature referred to bulk conditions. Intraparticle gradients under all conditions of operation at 26°C. were relatively small and the agreement between calculation and experiment about the same in all cases. On Figure 9a is an example for benzene feed concentration of 5.35%. The computed profiles agree fairly well with measured values although the former do not flatten as much near the center as measurements indicate.

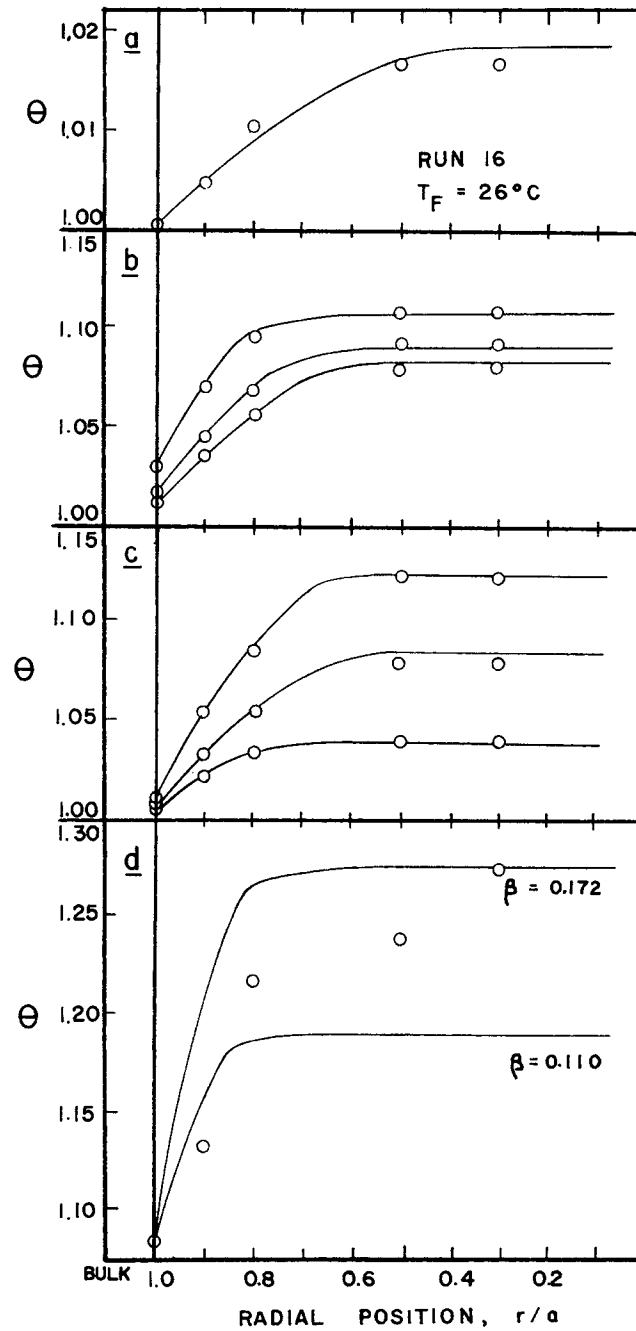

Fig. 9. Comparison of predicted and observed profiles for Pellet 1, T_F = 26 and 52°C. (a). Typical fit to data at 26°C. (b). Fit to feed flow change, compare Figure 4a. (c). Fit to feed concentration change, compare Figure 4b. (d). Fit to anomalous profile at high reaction rates, compare Figure 5c.

‡ It should be kept in mind that β here is defined with respect to bulk temperature and concentration conditions, $\beta = (C_B/C_S)(T_S/T_B)(\Delta T)_{max}/T_S$. Under experimental conditions, this is approximately $(\Delta T)_{max}/T_B$.

TABLE 2A. EXPERIMENTAL CONDITIONS OF RUNS SELECTED FOR ILLUSTRATION

	Run	Pressure, torr	H_2 flow $\times 10^3$, g.-mole/sec.	Mole %, H_2	Mole %, C_6H_6	T_F, °K.	T_B, °K.	Rate $\times 10^6$, g.-mole/(sec.)(g.)
Pellet 1:	8	768	7.39	97.7	2.23	299	299	0.151
	9	757	3.65	97.7	2.23		299	0.146
	10	757	11.11	97.7	2.23		299	0.145
	16	757	11.76	94.6	5.35	↓	301	0.240
	20	748	3.73	94.7	5.07	325	335	0.950
	21	761	7.61	95.4	4.45		331	0.820
	22	763	11.33	96.0	3.90		321	0.785
	23	760	3.87	89.2	10.13		341	2.690
	24	766	7.66	90.3	9.47		331	1.506
	25	766	11.60	90.4	9.46		321	1.250
	26	756	3.75	85.3	14.03		348	5.390
	27	756	7.70	85.6	13.48		333	2.258
	28	756	11.92	86.4	13.03	↓	328	1.573
	32	755	11.38	96.0	3.84	338	339	1.068
	33	755	7.45	95.1	4.71		343	1.390
	34	755	3.77	94.3	5.35		354	1.432
	35	757	11.51	92.5	7.35		340	1.680
	36	757	7.66	91.8	7.91		344	2.018
	37	757	3.68	89.7	9.47		358	2.730
	38	751	10.22	85.7	14.03		340	2.520
	39	751	7.86	83.7	15.59		358	4.710
	40	751	3.80	82.4	15.59	↓	374	6.950
Pellet 2:	205	760	7.76	85.6	14.32	340	347	2.360
	209	759	11.86	92.8	6.96	407	412	11.15
	210	759	3.79	81.1	17.39		438	26.32
	211	759	7.92	85.0	14.32		418	24.50
	212	759	12.58	80.0	19.50	↓	412	22.40
	217	761	7.92	83.8	16.16	328	333	1.160
	223	758	7.86	84.5	15.35	358	363	5.000

TABLE 2B. DIMENSIONLESS PARAMETERS OF RUNS SELECTED FOR ILLUSTRATION

	Run	φ	β	$\alpha \times 10^4$	γ	ξ	N_{Nu}	N_{Sh}	η (exp)	η (calc)
Pellet 1:	8	32.4	0.020	1.81	6.77	13.91	24.0	480	1.16	1.22
	9	32.4	0.020	1.81	6.77	13.91	17.1	343	1.12	1.13
	10	32.4	0.020	1.81	6.77	13.91	29.7	595	1.12	1.12
	16	32.5	0.048	4.33	6.71	13.77	29.7	595	1.56	1.29
	20	33.6	0.042	3.72	6.12	12.57	17.1	343	0.81	0.91
	21	33.7	0.037	3.28	6.12	12.57	24.0	480	0.87	0.88
	22	32.5	0.032	2.91	6.19	12.72	29.7	595	1.05	0.88
	23	35.6	0.083	7.24	5.94	12.20	17.1	343	1.77	1.56
	24	32.7	0.078	6.96	6.12	12.57	24.0	480	1.68	1.64
	25	31.6	0.078	7.05	6.19	12.72	29.7	595	1.77	1.74
	26‡	34.9	0.110	9.10	5.82	11.95	17.1	343	2.48	4.75
	27	32.4	0.110	10.26	6.08	12.49	24.0	480	2.37	2.37
	28	31.4	0.110	10.00	6.17	12.68	29.7	595	2.22	2.47
	32	36.0	0.025	2.77	5.99	12.31	29.7	595	0.73	0.63
	33	37.1	0.031	3.35	5.92	12.16	24.0	480	0.77	0.66
	34	38.6	0.034	3.75	5.84	11.99	17.1	343	0.46	0.57
	35	35.9	0.058	5.26	5.96	12.24	29.7	595	1.11	1.01
	36	36.8	0.058	5.61	5.90	12.13	24.0	480	1.09	1.00
	37	40.2	0.061	6.50	5.70	11.72	17.1	343	0.75	0.87
	38	34.6	0.100	11.95	5.96	12.24	29.7	595	1.90	1.92
	39‡	39.8	0.100	10.60	5.66	11.62	24.0	480	1.39	2.94
	40‡	44.9	0.100	10.20	5.41	11.12	17.1	343	1.02	4.11
Pellet 2:	205	20.3	0.008	10.10	5.84	11.99	2.4	720	1.17	1.14
	209	32.8	0.003	4.16	4.96	10.20	3.0	892	0.30	0.29
	210	36.3	0.006	10.26	4.62	9.50	1.7	515	0.34	0.38
	211	33.3	0.009	10.74	4.84	9.95	2.4	720	0.59	0.50
	212	29.5	0.012	15.86	4.93	10.12	3.0	892	0.76	0.69
	217	18.2	0.008	11.82	6.06	12.46	2.4	720	1.12	1.05
	223	23.0	0.006	10.30	5.58	11.46	2.4	720	1.16	1.02

‡ Parametric values for β determined from runs at similar conditions. For β from temperature rise measurements, the following parameters were determined:

26	27.9	0.172	9.10	5.82	11.95	17.1	343	2.48	2.05
39	30.8	0.168	10.60	5.66	11.62	24.0	480	1.39	1.37
40	37.2	0.147	10.20	5.41	11.12	17.1	343	1.02	1.41

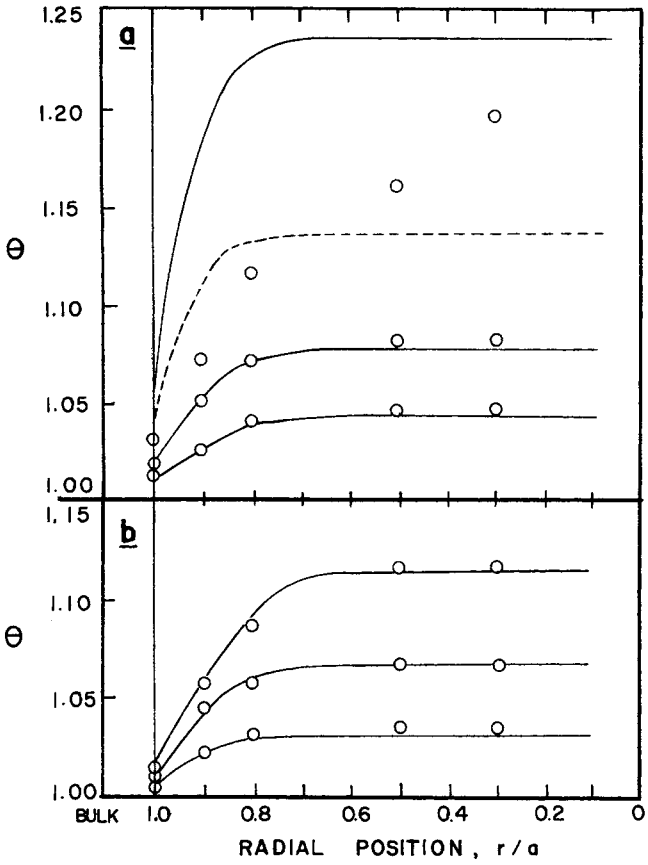

Fig. 10. Comparison of predicted and observed profiles for Pellet 1, $T_F = 65°C$. (*a*). Fit to feed concentration change at 10 liter/min. flow, compare Figure 5*b*. (*b*). Fit to feed concentration change at 15 liter/min. flow, compare Figure 5*a*.

Fits to the data of runs illustrated previously on Figure 4 for a feed temperature of 52°C. are shown on Figure 9b and c, treating variations of profiles with changes in flow and reactant composition. The agreement is excellent for all experiments at the two higher flow rates, and the interactions of internal and external gradients involving varying degrees of reaction zone penetration into the pellet described previously are quite well reproduced by the calculations. On Figure 9d, however, is shown the fit for Run 26, previously depicted on Figure 5c. Here the measured profile extended throughout the pellet interior and the overall intraparticle temperature rise was about 60°C. The upper profile in Figure 9d is computed with $\beta = 0.172$, corresponding to the measured temperature rise of 60°C., the lower profile was computed with $\beta = 0.11$, the value corresponding to the other two flow rates at this feed temperature and equivalent concentration levels (Runs 27 and 28) and also the value computed from individual measurements. Neither calculated profile is even qualitatively similar to that measured. It is believed that this anomalous behavior is due to a breakdown in the validity of the uniform boundary layer assumption; Maymo and Smith (*3*) reported some experiments in which the surface temperature of a spherical catalyst pellet was measured at different positions under reactive conditions. At low rates of reaction the temperature variation with position was less than 1°C., but in one run involving very high rates of reaction per volume of catalyst there was a 97°C. variation in surface temperature around the pellet circumference. It is probable that a similar situation existed in Run 26, where the measured rate of reaction was abnormally high—over twice that at identical conditions save flow rate in Run 27—and in several other runs involving low flow rate and high feed concentration such as Runs 39 and 40 at 65°C. In all such cases steeply ascending profiles extend throughout the pellet and computed results based on the two differing β values as described are not even qualitatively similar in shape. The system was shown not to exhibit hysteresis in a number of perturbation experiments under the conditions reported here (*13*), so it does not appear that such results are due to the existence of multiple stable reaction states.

The fit to a series of runs at 65°C. showing directly both the development of the anomalous profile and the excellent agreement obtained at the same conditions but higher flow rates is given on Figure 10a; excellent agreement of calculation with experiments on feed composition variation and temperature change is generally obtained as shown on Figures 10b and 9c.

In summary, the steady state gradients both internal and external are well described by the calculations for all the experiments reported here except those involving low convective transport rates and high reaction rates, under which conditions it seems probable that nonuniformities develop in the boundary layer and the computational model fails. For Pellet 2, in which intraparticle conditions were found experimentally to be isothermal in all experiments, the calculation is in excellent agreement, within about 1°C., in all cases. Since these profiles are all flat, no separate figures for the results with Pellet 2 are given here.

Catalytic Effectiveness

The effectiveness factor was computed from Equation (5) for each run and compared with the experimental value determined from the ratio of observed rate to that computed from Equation (1) for bulk conditions. These results are shown on Figure 11 for all experiments conducted with both pellets. With a few exceptions the deviation between observed and predicted values is less than 15%. For Pellet 2 the only rate enhancement is due to the boundary layer temperature rise since the interior is isothermal. This is not sufficient to outweigh the mass diffusion resistance so effectiveness factors are unity or less. For Pellet 1, however, there are in a number of cases sub-

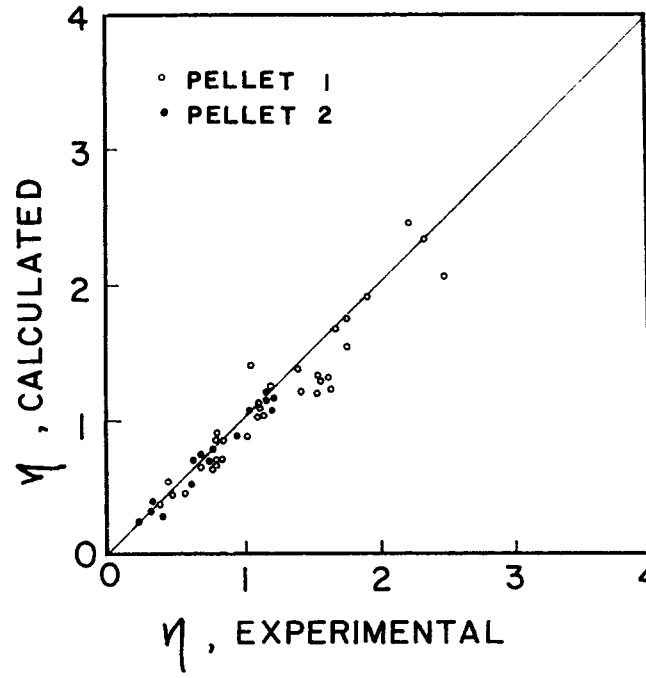

Fig. 11. Summary of measured and calculated effectiveness factors for all runs.

stantial internal gradients in combination with external gradients and many of the corresponding effectiveness factors are greater than unity.

For experiments in which large deviations from the predicted temperature profiles were observed, two calculated values of η are reported in Table 2 corresponding to the two β values described. The η corresponding to the β value extracted from observed temperature rise is far higher than observed effectiveness, but that for the lower β value is in reasonably good agreement with observation. This somewhat surprising result is in line with the observation of Rosner (*15*), who has discussed some cases in which the uniform boundary layer approach yields respectable predictions of overall effectiveness while failing in the computation of profiles.

CONCLUSIONS

The behavior of this catalytic system is generally well predicted by the one dimensional heat and mass diffusion model, where all the parameters are separately determined, as written to include intraparticle and boundary layer graidents. Siginficant intraparticle graidents do exist in exothermic catalysis under moderate conditions of operation at least; the ratio of Sherwood to Nusselt numbers for Pellet 1 (≈ 20) is not sufficiently large to cause the entire thermal gradient to exist in the boundary layer. For Pellet 2, however, this ratio is more than an order of magnitude larger due to the increased thermal conductivity and the simplification of isothermal intraparticle conditions, as envisioned by McGreavy and Thornton (*9*) for highly exothermic systems, is obeyed. The rather complex interaction between internal and external gradients is well represented by the computation, and the parametric values herein determined are in agreement with one of the limiting cases reported previously for this system (*1*).

The measured temperature profiles are radially symmetric and do not exhibit minima in the pellet interior as reported in measurements (*1, 5*) in an alternative single pellet reactor. Such minima are apparently due to nonuniform axial temperature fields and accompanying conduction effects.

The development of very steep, apparently asymmetric gradients was associated with several experiments in which convective transport rates were relatively small and reaction rate was high. In view of the similar experience of Maymo and Smith (*3*) and the predictable behavior of the system at identical conditions but higher N_{Sh} and N_{Nu} it is felt that such observations are due to the development of nonuniform boundary layers in the single pellet reactor at the lowest flow rates employed. The corresponding experimental conditions are somewhat more severe than those envisioned by Bischoff (*16*) in a recent analysis of the effects of anisotropic external fields, so it is not clear whether such events would be of importance in the actuality of a fixed bed reactor. The effects are quite large, though, so the question may merit more detailed examination.

ACKNOWLEDGMENTS

This research was principally supported by the National Science Foundation. We should also like to acknowledge the financial aid of Yale University, Chevron Research Company, and the Institute for Industrial Research and Standards of Ireland. Progress of the research was materially and morally assisted at various points by Harding Bliss, C. O. Bennett, and V. W. Weekman, Jr.

NOTATION

a = pellet radius
A, B = constants, Equation (1)
C = concentration of benzene
c_p = heat capacity
D = diffusivity
E = activation energy
h = heat transfer coefficient
H = heat of adsorption of benzene
ΔH = heat of reaction
k_m = mass transfer coefficient
N_{Nu} = Nusselt number
N_{Sh} = Sherwood number
r = radial distance
P = pressure
R = gas constant
T = temperature
X = mole fraction
y = dimensionless concentration, $y \equiv C/C_B$
z = dimensionless distance, $z = r/a$

Greek Letters

α = parameter of dimensionless rate equation, $\alpha \equiv BC_B$
β = thermicity parameter, $\beta \equiv C_B D_e(-\Delta H)/\lambda_e T_B$
γ = activation energy parameter, $\gamma \equiv E/RT_B$
δ = diffusion modulus, $\delta = a^2 A \exp(-E/RT_B)/D_e$
ϵ = porosity
ξ = heat of adsorption parameter, $\xi = H/RT_B$
η = effectiveness factor, Equation (5)
θ = dimensionless temperature, $\theta = T/T_B$
λ = thermal conductivity
ρ = density
τ = ratio of N_{Sh} to N_{Nu}
φ = Thiele modulus, $\varphi^2 = \delta$

Subscripts

B = bulk conditions, benzene
e = effective property
F = feed conditions
G = gas phase
H = hydrogen
S = surface

LITERATURE CITED

1. Irving, J. P., and J. B. Butt, *Chem. Eng. Sci.*, **22**, 1859 (1967).
2. Miller, F. W., and H. A. Deans, *AIChE J.*, **14**, 45 (1967).
3. Maymo, J. A., and J. M. Smith, *AIChE J.*, **12**, 845 (1966).
4. Wurzbacher, C., *J. Catalysis*, **5**, 476 (1966).
5. Hughes, R., and H. P. Koh, *Chem. Eng. J.*, **1**, 186 (1970).
6. Carberry, J. J., *Ind. Eng. Chem.*, **58**, 40 (1966).
7. Hatfield, B., and R. Aris, *Chem. Eng. Sci.*, **24**, 1213 (1969).
8. Kehoe, J. P. G., and J. B. Butt, *ibid.*, **25**, 345 (1970).
9. McGreavy, C., and D. M. Thornton, *ibid.*, 303 (1970); D. L. Cresswell, *ibid.*, **24**, 608 (1969).
10. Cresswell, D. L., *ibid.*, **25**, 267 (1970).
11. Petersen, E. E., *ibid.*, **17**, 987 (1962).
12. Kehoe, J. P. G., and J. B. Butt, *J. Appl. Chem. Biotechnol.* (in press).
13. Kehoe, J. P. G., Ph.D. dissertation, Yale University, New Haven, Conn. (1971).
14. Foster, R. N., J. B. Butt, and H. Bliss, *J. Catalysis*, **7**, 179 (1964).
15. Rosner, D. E., *AIChE J.*, **9**, 321 (1963).
16. Bischoff, K. B., *Chem. Eng. Sci.*, **23**, 451 (1968).

Manuscript received August 17, 1971; revision received October 1, 1971; paper accepted October 11, 1971.